

Military Technical College  
Kobry Elkobbah, Cairo,  
Egypt.



4<sup>th</sup> International Conference  
On  
Chemical & Environmental  
Engineering  
27-29 May 2008

## SYNTHESIS, CHARACTERIZATION AND APPLICATION OF POLYANILINE-ORGANOCLAY NANOCOMPOSITES

N. Salahuddin\*, M. M. Ayad\*\* and M. Ali\*\*\*

### ABSTRACT

Polyaniline (PANI) - organoclay nanocomposites were prepared by intercalation of aniline monomer into montmorillonite (MMT) modified by polyoxyalkylene followed by subsequent oxidative polymerization of the aniline in the interlayer spacing. The organoclay was prepared by cation exchange process between sodium cation in MMT and  $\text{NH}_3^+$  in four different types of polyoxyalkylene diamine and triamine with different molecular weight. Infrared spectra (IR) confirm the electrostatic interaction between the positively charged group ( $\text{NH}_3^+$ ) and the negatively charged surface of MMT. The absence of  $d_{001}$  diffraction band in the nanocomposites was observed at certain types and contents of organoclay. Scanning electron microscopy (SEM) and transmission electron microscopy (TEM) were employed to determine the dispersion of the clay into PANI. PANI chains in the nanocomposites are more thermally stable than pristine PANI. This improvement is attributed to the presence of nanolayers with high aspect ratio acting as barriers, thus shielding the diffusion of degraded PANI from the nanocomposites. The electrical conductivity of the nanocomposites was increased 30 times more than that of pure MMT at certain concentration. PANI-organoclay nanocomposites were used as curing agent for epoxy resins. IR and Differential Scanning Calorimetry (DSC) confirm the curing of epoxy. The absence of  $d_{001}$  diffraction band of organoclay in the nanocomposites was observed by X-ray diffraction (XRD). The structure argument was further supported by TEM. Electrical conductivity of the nanocomposites within the range  $2.1 \times 10^{-7} - 3.2 \times 10^{-7}$  S/cm depending on the concentration of the PANI-organoclay.

### KEYWORDS

Nanocomposites, montmorillonite, polyaniline

---

\* Assistant professor of physical chemistry, Chemistry Department, Faculty of Science, Tanta University

\*\* Professor of physical chemistry, Chemistry Department, Faculty of Science, Tanta University

\*\*\* Graduate student, Department of Chemistry, Faculty of Science, Tanta University.

## INTRODUCTION

PANI is one of the most technologically important materials because of its environmental stability in conducting form, low cost of synthesis and high conductivity. These properties provide possible applications in battery electrodes [1,2], electrochromic devices [3,4], energy storage devices [5], photoelectric cell [6] and anticorrosion. However, the major problems related to its successful utilization, lies in its poor mechanical properties, process ability and its insoluble nature in common organic solvents, make PANI unsatisfactory for practical applications. Many attempts have been made to improve these aspects by blending the PANI with thermoplastics [7-10] and thermosetting polymers [11].

Epoxy (EP) resins are widely used in coatings and structural applications [12], because the thermosetting polymer can be tailored to suit specific performance characteristics. As a result of their high cross-link density and aromatic backbone, most EP resins are rigid materials and fail by brittle fracture [13]. For the preparation of conductive PANI/EP resin composites, usually doped PANI is blended with EP resin. Specific plasticizer is used to assist dispersion of the conductive polymer; meanwhile, basic curing agents should be avoided in order to avoid de-doping effects. Peltola *et al.* [14] prepared PANI-camphor sulfonic acid/EP resin composites in the presence of alkyl phenol, using a BF<sub>3</sub> based curing agent. Jeevananda *et al.* [15] prepared PANI/EP novolac resin through polymerization of aniline in dichloromethane solution of the resin. Because doped PANI could be de-doped by amines and other alkaline substances, the curing agent should be selected carefully to avoid negative effects of the chemicals and curing temperatures on the doping level.

Interaction between layered silicate materials and polymers has attracted interests. Dispersion of layered silicate in the polymers has resulted in enhancements of mechanical and thermal properties of the matrix at unexpectedly small inorganic contents [16,17]. Layered silicate-polymer nanocomposites have been prepared using an incredibly wide range of polymers [18-25]. Four general methods have been reported for preparing PANI/clay nanocomposites [26-30]. The first one consists of the use of transition metal ions (Cu<sup>+2</sup>) introduced as exchangeable cations into homoionic smectite to induce direct topotactic PANI formation [31]. The second procedure is based on the previous exchange of the interlayer cations (Na<sup>+</sup>) by anilinium species, which are subsequently polymerized by means of an oxidizing agent such as APS [32]. The third method involves the addition of PANI to the reaction media in which the clay is hydrothermally synthesized [33]. Finally, the fourth method is emulsion polymerization, in which the emulsifier in emulsion system contributes to maximization of the affinity between hydrophilic host (clay) and hydrophobic guest (aniline) [34]. In this work, an exfoliated PANI-organoclay was prepared by *in situ* polymerization of aniline using (2-50 wt%) organoclay. Then, nanocomposites are used as curing agent for EP resin. The structure of the cured materials was studied by IR, DSC, XRD, SEM and TEM. Electrical and thermal properties were measured and the resultant composites may find application as an antistatic material.

## EXPERIMENTAL

### Chemicals

The clay used in this study was MMT from Southern Clay products Inc. (Gonzales, Texas, USA) under the trade name of mineral colloid. The reported cation exchange capacity (CEC) was 114.8 m.eq/100 g. The  $d_{001}$  (interlamellar or interlayer) spacing is 9.6 Å. Polyoxypropylene diamine, Jeffamine D<sub>230</sub>, (D<sub>230</sub>) having an average molecular weight of 230 and the primary amine content is 8.3 meq/g; Polyoxypropylenetriamine, Jeffamine T<sub>403</sub>, (T<sub>403</sub>) having an average molecular weight of approximately 440 and primary amine content is 6.1 meq/g; Polyoxyethylenediamine, which are aliphatic primary diamines structurally derived from propylene oxide-capped polyethylene glycol, under the trade name of Jeffamine ED<sub>600</sub> (ED<sub>600</sub>) and Jeffamine ED<sub>900</sub> (ED<sub>900</sub>) with different molecular weights 600 and 900 and amine content 3.19, 2.05 meq/g respectively were obtained from Huntsman Corporation (Austin, USA). Aniline was purified by vacuum distillation. APS (B.D.H.) was used as received. Standard, general purpose EP resin D.E.R.331 (EP equivalent weight is 186-190) based on diglycidyl ether of bisphenol A (DGEBA) was obtained from Dow Chemical Japan Ltd.

### Preparation of organoclay

The organoclay was prepared by a cation-exchange reaction between the sodium cations of MMT clay and  $\text{NH}_3^+$  groups in Jeffamines. Typically, 10 g of MMT was suspended in 300 ml distilled water and stirred for 3 h at 60 °C followed by stirring overnight at room temperature. An aqueous solution of 2.8 g of acidified D<sub>230</sub> with HCl aqueous solution was added to the swelled clay with constant stirring. The mixture was then stirred for an additional 24 h. The precipitate was filtered and washed with water several times, until no chloride ions were detected in the filtrate by testing with  $\text{AgNO}_3$ . The resultant product (I) was dried at 60 °C to give 7.134 g. The same procedure was followed for the other types of Jeffamines, Table (1).

### Preparation of PANI/organoclay nanocomposites by *in situ* polymerization

As a typical procedure for the preparation of the PANI/D<sub>230</sub>-MMT nanocomposite materials. 0.9 g of aniline was added to 0.0183 g of D<sub>230</sub>-MMT (I) swelled in 5 ml DMF and stirred for 24 h at room temperature followed by stirring for 3 h at 60 °C. The mixture was cooled to 0 °C. APS (2.2 g) dissolved in 50 ml 0.1 M HCl was added drop wise and polymerization continued for 24 h. The molar ratio between aniline and APS was 1 and the concentration of aniline was 0.18 M/L. The dark green precipitate (I<sub>a</sub>) was washed with a large amount of 0.1 M aqueous HCl solution several times and with methanol. The product was filtered and dried at 50 °C. For the sake of comparison, different types and different contents (2-50 wt. %) of organoclays have been used to prepare PANI/organoclay nanocomposites as shown in Table (2).

### **preparation of pristine PANI**

Aniline was oxidized with APS in 0.1 aqueous HCl medium. The polymerization was started by mixing the reactants at 20°C. After 3 h, the precipitate of PANI hydrochloride was collected by filtration, then washed with 0.1M hydrochloric acid and dried at 60°C in vacuum oven.

### **Preparation of PANI/D<sub>230</sub>-MMT/EP nanocomposites**

PANI/D<sub>230</sub>-MMT/EP nanocomposites were prepared by first swelling the desired concentration of dry modified PANI/D<sub>230</sub>-MMT with chloroform for 8h. The swelled materials were subsequently stirred into the appropriate amount of EP resin for 8 h in order to allow the diffusion of EP resin molecules between the layers. The swelled materials were then degassed for approximately 20 min in a vacuum oven until bubble free. Different amount of EP resin and PANI/D<sub>230</sub>-MMT nanocomposites were used for each formulation (Table 3). The mixtures were poured into a preheated open rectangular glass mold with dimension 60 mm x 80 mm and 5 mm thickness having silicon rubber spacer, followed by removing air bubbles using vacuum pump. The surface of the glass was pretreated by dichlorodimethylsilane. The molds were then cured at 160°C for 24 h. The same procedure was followed using pristine PANI as curing agent for EP (Table 3).

### **Doping of PANI/EP and PANI/D<sub>230</sub>-MMT/EP nanocomposites**

The cured samples of PANI/EP and PANI/D<sub>230</sub>-MMT/EP nanocomposites were dipped in 1M HCl solution for 48 h. The samples were dried at room temperature for 12 h and under vacuum for 3 h.

## **RESULTS and DISSCUSION**

The synthetic procedure used for nanocomposite preparation is essentially developed by Usuki *et al.* for nylon-silicate nanocomposite [25]. It involves dispersion of the organically modified clay in a suitable monomer followed by polymerization. A similar synthetic protocol in the present study was used in the preparation of PANI/MMT nanocomposites. This involved mixing of clay modified by Jeffamines with aniline monomer in the presence of suitable solvent followed by addition of oxidizing agent to initiate polymerization between the layers. Under proper conditions, exfoliation of the organoclay into individual silicate layers occurs, which ultimately becomes dispersed within the macromolecular matrix. These samples were mixed with EP resin using good solvent and cured. The role of D<sub>230</sub> in organoclays is to lower the surface energy of the inorganic host and improve the wetting characteristics with the polymer. In addition, it could provide functional groups that can initiate curing of EP resins to improve the strength between the inorganic and polymer matrix.

## Characterization of PANI/organoclay nanocomposites

Fig. (1) shows IR spectra of organoclay D<sub>230</sub>-MMT (I), pure PANI and PANI/D<sub>230</sub>-MMT (I<sub>a</sub>) nanocomposite. Characteristic bands corresponding to MMT in organoclay are shown at 1044 cm<sup>-1</sup> ( $\nu$  (Si-O)), 919 cm<sup>-1</sup> ( $\delta$  (Al-OH)) and 520 cm<sup>-1</sup> ( $\nu$  (Si-O-Al)). The band at 1461 cm<sup>-1</sup> can be assigned to stretching (C-N), while bands at 3423 cm<sup>-1</sup>, 1632 cm<sup>-1</sup> can be attributed to the N-H stretching and bending modes of the NH<sub>3</sub><sup>+</sup> group [35, 36] confirming the presence of ionic bond between D<sub>230</sub> and MMT.

The characteristic vibration bands for PANI are shown in Fig. (1) The broad band at 3441 cm<sup>-1</sup> is due to the characteristic free N-H stretching vibration, which suggests the presence of secondary amino groups (-NH-). The weak band at 2921 cm<sup>-1</sup> arises from the aromatic C-H stretching vibration. The characteristic band appearing at 1477 cm<sup>-1</sup> corresponds to the benzenoid ring stretching frequency and the peak appearing at 1579 cm<sup>-1</sup> corresponds to the quinoid ring stretching frequency. The absorption band at 1293 cm<sup>-1</sup> is due to C-N stretching vibration of secondary aromatic amine. The band characteristic of the conducting protonated form is observed at 1238 cm<sup>-1</sup>. It has been interpreted as C-N<sup>+</sup> stretching vibration in the polaron structure. The 1124 cm<sup>-1</sup> band can be assigned to a vibration mode of the -NH<sup>+</sup>= structure, which is formed by protonation. The broad nature of this peak is due to the high degree of electron delocalization which was expected because of the greater degree of oxidation. The C-H out-of-plane bending vibration band of 1,4-disubstituted benzene ring appears at 796 cm<sup>-1</sup>. These observed bands are in good agreement with previously published values [26]. It was reported that there are physical interactions between the intercalated PANI and MMT [29]. As can be seen, the clay band dominates IR spectra at 1044 cm<sup>-1</sup> in the composite, making the analysis of this spectral region difficult. IR spectra of the composite show characteristic bands of pure PANI indicating the existence of PANI in the emeraldine salt (ES) form. Comparing the free PANI with PANI/D<sub>230</sub>-MMT(I<sub>a</sub>) nanocomposites, it is noticed that the characteristic band for C-N stretching in the free PANI have their counterpart band in the nanocomposites spectra, indicating that the same kind of polymerization occurs inside the gallery. However, it is worth noting from a closer look at the spectra that there is a shift of the band at 1293 cm<sup>-1</sup> that assigned as stretching vibration of ( $\nu$  (C-N)) to 1298 cm<sup>-1</sup>. The frequency shift of ( $\nu$ (C-N)) observed in this composite is due to physical interaction between PANI chain and silicate layers. In addition, the band at 1238 cm<sup>-1</sup> in PANI that attributed to C-N<sup>+</sup> stretching vibration in the polaron structure shifts to 1247 cm<sup>-1</sup> in PANI/D<sub>230</sub>-MMT. This indicates that the electrostatic interaction between the positive charge of PANI and the negatively charged surface of the clay layers affects the vibrational motion of PANI.

XRD pattern of the clay modified by D<sub>230</sub>, T<sub>403</sub>, ED<sub>600</sub>, and ED<sub>900</sub> was shown in Figs (2-5). The organoclay powders showed a strong diffraction peak with a characteristic interlayer spacing of 14 and 14.7 Å for D<sub>230</sub>, T<sub>403</sub> respectively, that was very close to the reported spacing [23]. Clay modified by ED<sub>600</sub>, ED<sub>900</sub> showed a sharp peak with a spacing of 17.3 Å and a broad peak with a spacing of 17.6 Å, respectively. Taking into account a layer thickness of 9.3 Å, the basal spacing of 14, 14.7, 17.3 and 17.6 Å corresponds to a gallery height of 4.7, 5.4, 8.0 and 8.3 Å, respectively. The peak appears at large angle ( $2\theta=20^\circ$ ) in all the diffraction patterns corresponds to the

crystallographic plane (110) and (020) of the clay layers. The presence of this peak demonstrates that the XRD analysis is sensitive enough to detect the presence of the clay in the composites [37].

The peak characteristic to D<sub>230</sub>-MMT and T<sub>403</sub>-MMT was disappeared in PANI/organoclay nanocomposites with different concentration of D<sub>230</sub>-MMT and T<sub>403</sub>-MMT. This indicates that almost complete exfoliation of the silicate layers takes place, and a nanocomposite structure was obtained. A notable small broad diffraction peak at  $2\theta = 4.2^\circ$  ( $20.5\text{\AA}$ ) was appeared. This peak was observed in pure PANI. However, In PANI/organoclay nanocomposites using ED<sub>600</sub>, it was noted that intense XRD signals from organoclay peaks are apparent in nanocomposites containing 50 wt % organoclay. When the amount of organoclay decreases (25 and 14 wt %), the peak characteristic to the organoclay disappeared and broad peaks appeared at  $2\theta$  equals  $6^\circ$ . If the nanocomposites contains 2 wt % of organoclay, the peak disappeared. The intercalation of more polymer chain inside clay layers lead to disordering of the layered clay structure. Similar behavior was obtained for PANI/organoclay using ED<sub>900</sub>, Fig. (5), except that the broad peaks of the organoclay were slightly shifted to lower  $2\theta$ . The inefficient exfoliation of MMT in these two systems at high concentration was related to the swelling properties of organoclay in DMF. This indicates that the type and the molecular weight of the polyoxyalkylene used in modification of the clay affect the morphology of the resulting material. It is worth mentioning that many studies on PANI/clay nanocomposites have been carried out, and an intercalated structure were obtained [38,39]. The basal spacing of PANI/smectite clay nanocomposites was varied from 13 to 15  $\text{\AA}$  depending on the experimental conditions in the polymerization of aniline species. It was assumed that the rings in a pseudoplanar or tilted arrangement with respect to the (a, b) silicate plane. However, Porter *et al.* [39] has claimed the possible formation of mono- and bilayers of PANI in the interlayer regions of clays.

To more clearly identify exfoliated structure of the nanocomposites, TEM images of the PANI/D<sub>230</sub>-MMT at different concentrations were shown in Fig. (6). Dark stripes represent the clay layers and the gray/white area represents the polymer matrix [28]. At low concentration, TEM images of PANI/D<sub>230</sub>-MMT show nanosized clay domains with an average size of 150 nm (Fig. (6(a))). On the other hand, The TEM of the composites at high concentration of organoclay has a considerable amount of stacked layers with an average size of 250 nm in which polymer chains are intercalated as evidence from XRD (Fig. (6(b))).

It was reported that the elementary building block of the composite may erect an aggregate of a micro scale [40] or a nanostructure [20]. SEM images of PANI and PANI/D<sub>230</sub>-MMT nanocomposites are shown in Fig. (7). The microstructure of PANI particles was compared with that of the composites. It can be seen that the PANI particles Fig. (7(a)) have a spherical shape with porous structure. The average diameter of PANI is 200 nm. In case of PANI/D<sub>230</sub>-MMT nanocomposites Fig. (7(b, c)), it is worth noting that examination of the fractured surface did not reveal inorganic aggregation, indicating that the mineral domains are homogenously dispersed in the

polymer matrix. At high magnification, both plate-like structure and spherical particles are shown. It can be easily assumed that spherical particles are pure PANI. The plate-type particles represent a hybrid of PANI and clay particles, which was formed during the polymerization step. The spheroidal morphology typical of the neat PANI is hardly observable in the presence of high D<sub>230</sub>-MMT content, and plate-like particles are noticed. It should also be noted that most of the PANI chains are intercalated into the interlayer spacing of MMT as shown in XRD data. However, in case of 2 wt % of D<sub>230</sub>-MMT free PANI particles can be clearly seen.

### Characterizations of PANI-D<sub>230</sub>-MMT/ EP nanocomposites

The IR absorption, Fig. (8) at 916 cm<sup>-1</sup> in EP resin is attributed to the stretching absorption of C-O in the epoxide ring. This absorption clearly disappeared by curing at 160°C in all PANI/D<sub>230</sub>-MMT/EP nanocomposites. This confirmed the curing of EP by PANI and the formation of the network structure. In addition, the band at 3100 cm<sup>-1</sup> that was assigned to terminal Q=NH in PANI and PANI/D<sub>230</sub>-MMT was disappeared when they are added to EP matrix, which indicates the molecular level interaction of PANI chains with EP could be achieved.

DSC thermograms (Fig (9)) of the first run of PANI/EP and PANI/D<sub>230</sub>-MMT/EP does not show exothermic peak. This behavior confirmed the curing of EP and formation the network structure. The large DSC endothermic peak in Fig (9) for PANI/EP between 100 and 190°C correlates with the elimination of HCl dopants [41]. It was reported that the glass transition temperature T<sub>g</sub> of the neat EP matrix is 113°C and for PANI at 140°C [42]. However, the T<sub>g</sub> appears at 82, 91°C for EP cured with PANI and PANI/D<sub>230</sub>-MMT, respectively. The reduction in T<sub>g</sub> was suggested to be due to the inhibition of curing reaction by presence of PANI. Tsotra *et al.* [11] reported that the T<sub>g</sub> decreases slightly with the addition of the conductive salt PANI in the EP matrix. The glass transition temperature is a parameter that can be used to indicate the differences in the degree of cure. With decreasing crosslinking, the freedom of movement in the polymer network increases. As a result, T<sub>g</sub> is shifted to lower temperatures.

XRD pattern of PANI/EP is presented in Fig. (10). It exhibits a broad peak at 2θ=5.4°. This indicates that the sample contained a marginal fraction of a crystalline phase. PANI/D<sub>230</sub>-MMT/EP nanocomposites do not show any peaks characteristic to D<sub>230</sub>-MMT. Interestingly, the characteristic peak for PANI/EP at 5.4° seems to be broader in the presence of clay. Probably the interactions of PANI with the clay layers disrupt the ordered structure of PANI/EP.

The morphology of the PANI/D<sub>230</sub>-MMT/EP nanocomposite was detected by TEM. A typical TEM micrograph for cured EP matrix using PANI/D<sub>230</sub>-MMT is given in Figs. (11). The nanodomains with an average thickness size of 300 nm was dispersed in PANI/EP matrix. It is apparent the compatibility of PANI with the EP matrix with no phase separation.

## Properties of Nanocomposites

Fig. (12(a)) depicts TGA thermograms of the D<sub>230</sub>/MMT, PANI, and PANI/D<sub>230</sub>-MMT nanocomposites. There are four major stages of weight loss for the organically modified clay (D<sub>230</sub>/MMT). The first weight loss below 100 °C is a result of the release of free water. The second and third stages in the temperature range of 200–600 °C are associated with the decomposition of the intercalated polyoxypropylene in the organoclay. In the last stage of weight loss in the temperature range of 600–780 °C, the structural water that is bonded to hydroxyl groups start to decompose and is being released. For pure PANI, a small weight loss around 100 °C is presumably due to the elimination of water and other volatiles (HCl vapors). The weight loss occurring between 200 and 400 °C (60 wt %) is approximately the weight fraction of dopant. Above 400 °C, the polymer itself decomposes. The TGA thermogram of PANI/D<sub>230</sub>-MMT nanocomposite (I<sub>c,d</sub>) containing 25,50 wt% D<sub>230</sub>-MMT and PANI/organoclay nanocomposites (II<sub>b</sub>, III<sub>b</sub>, IV<sub>b</sub>), Fig. (12(b)) confirms the thermal stability. There is no sharp weight loss between 380 and 400 °C as observed in PANI. This behavior is expected because the clay platelets protect and delay the intercalated chains from undergoing a degradation process. As the amount of D<sub>230</sub>-MMT increased, the total weight loss of the nanocomposite decreased. It is suggested that, for the nanocomposites, the silicate layers (nanolayers) with a high aspect ratio (100–1000) are believed to effectively act as barriers, blocking the degradation of PANI chains located between the interlayer spacing. The room temperature conductivity ( $\sigma_{RT}$ ) of PANI/organoclay nanocomposites varies from  $5 \times 10^{-6}$  to  $3.72 \times 10^{-2}$  S/cm. There exists an increase in  $\sigma_{RT}$  in PANI composites with increasing PANI content, as shown in Fig. (13). The presence of high content of free PANI chains facilitate the electron transfer between the intercalated PANI chains, presumably because of the connectivity of free PANI chains. These composites result from the assembly of a conducting polymer separated by individual silicate layers of insulating character. Moreover, electrical transport through short and narrow intercalated polymer chains is strongly disfavored. The constrained polymer in the intracrystalline region can impose chain conformation changes that also contribute to a decrease in the conductivity of the system. Interestingly the conductivity of EP cured with PANI is lower than  $10^{-9}$  S/cm (Table 3). However, upon using the PANI/D<sub>230</sub>-MMT nanocomposites the conductivity take the range from  $1.7 \times 10^{-7}$  to  $3.2 \times 10^{-7}$  S/cm depending on the percentage of PANI. Tsotra *et al.* [11] proved that the dispersion quality of PANI was strongly related to the final electrical properties of the cured blends. PANI morphologies should be responsible for the dispersion of PANI and the formation of conductive path. They explained that the poor dispersion of PANI in EP leads to the creation of agglomerates which are mostly surrounded by the insulating matrix and unable to come into contact with each other. However, a very fine network results in enhancement electrical properties.

## CONCLUSION

A series of PANI/organoclay nanocomposites have been prepared by the intercalation of aniline monomer into interlayer spacing of MMT modified by different molecular weight of polyoxyalkylene followed by in situ oxidative polymerization of aniline monomers. It is evident from IR spectra that there are electrostatic

interactions between the PANI chains and the MMT layers. It is observed from XRD studies that the peak characteristic to  $d_{001}$  was disappeared in PANI/organoclay nanocomposites at certain types and contents of organoclay. SEM and TEM observations suggest that PANI mineral lamellae are assembled to form nanodomains, whose average size was 150 and 250 nm depending on the organoclay content. EP resin was cured using PANI and two different ratios of PANI/D<sub>230</sub>-MMT nanocomposites. It is evident curing of EP from IR spectra and DSC measurements. It is observed from XRD studies that the peak characteristic to  $d_{001}$  of organoclay was disappeared in PANI/D<sub>230</sub>-MMT/EP nanocomposites. TEM observations suggest that nanodomains whose average size was 300 nm was dispersed in the PANI/EP matrix. Based on the TGA analysis, the PANI chains in the PANI/organoclay nanocomposites are more thermally stable than those of pure PANI. The room temperature conductivity of PANI/organoclay nanocomposites varies from  $5 \times 10^{-6}$  to  $3.72 \times 10^{-2}$  S/cm depending on the amount of PANI in the nanocomposites. Conductive EP composite containing PANI layered silicate had higher conductivity by comparison with that containing pure PANI.

## REFERENCES

- [1] MacDiarmid A. G., Mu S. L., Somasiri N. L. D., Wu W., *Mol Cryst Liq Cryst* **121**, 187(1985).
- [2] Novak P., Muller k., Santhanam K. S. V., Hass O. , *Chem Rev*, **97**,207(1997).
- [3] Kobayashi T., Yonevama N., Tamura H., *J Electroanal Chem*, **177**, 281(1984)
- [4] Batich C. D., Laitinen H. A., Zhou H. C. *J Electrochem Soc*, **137**,883(1990) .
- [5] Trinidal F., Montemayor M. C., Falas E., *J Electrochem Soc* ,**138**, 3186(1991).
- [6] Dong Y. H.,. Mu S. L, *Electrochim Acta*, **36**, 2015(1991).
- [7] Hu H., Saniger J. M., Banuelos J. G., *Thin Solid Films*, **347**, 41(1999).
- [8] Cao Y., Paul S., Heeger A. J., *Synth Met*, **48**, 91(1992) .
- [9] Heeger A. J., *Trends Polym Sci* , **3**, 39 (1995).
- [10] Pud A., Ogurtsov N., Korzhenko A., Shapova G.I., *Prog Polym Sci*, **28**, 1701(2003)
- [11] Tsotra P., Gryschuk O., Friedrich K., *Macromol Chem & Phys*, **206**, 787(2005).
- [12] Ellis B., *Chemistry and Tecnology of Epoxy Resins*, Blackie Academic&Professional, New York (1993).
- [13] Kinloch A. J., *Structural Adhesives, Development in Resins and Primers*, Elsevier, New York (1986).
- [14] Peltola J., Cao Y., Smith P., *Adhes Age*, **38**, 18 (1995)
- [15] Jeevananda J., Palaniappan S., Siddaramaiah H., *Appl Polym Sci*, **74**, 3507 (1999).
- [16] Patel H., Somani R. S., Bajaj H. C., Jasra, R. V. B. *Mater Sci*, **29** , 133 (2006).
- [17] Pinnavaia T. J., Beall G. W., *Polymer-Clay Nanocomposites*. Wiley: New York (2000).
- [18] Moet A., Akelah A., Hiltner A., Baer E., *Mater Res Soc Symp Proc*, **351**, 91 (1994).
- [19] Salahuddin N., Shehata M., *Polym*, **42**, 8370 (2001).
- [20] Akelah A., Salahuddin N., Hiltner A., Baer E., Moet A., *Nanostructured Mater*, **4** , 965 (1994) .

- [21] Akelah A., Salahuddin N., Hiltner A., Baer E., Moet A., *Mater Lett*, **22**, 97 (1995).
- [22] Salahuddin N., Moet A., Hiltner A., Baer E., *Eur Polym J*, **38**, 1477(2002).
- [23] Salahuddin N., *Polym Adv Technol*, **15**, 251(2004).
- [24] Salahuddin N., Rehab A., *Polym Int*, **52**, 241(2003).
- [25] Usuki A., Kojimai Y., Kawasumi M., Okada A., Fukushima Y., Kurauchi T., Kamigaito O., *J Mater Res*, **8**, 1179 (1993).
- [26] Nascimento G. M. do, Constantino V. R. L., Landers R., Temperini M. L. A., *Macromolecules*, **37**, 9373 (2004).
- [27] Nascimento G. M. do, Constantino V. R. L., Temperini M. L. A., *Macromolecules*, **35**, 7535 (2002).
- [28] Bae W. J., Kim K. H., Jo W. H., *Macromolecules*, **37**, 9850 (2004).
- [29] Lee D., Char K., Lee S. W., Park Y. W., *J Mater Chem*, **13**, 2942 (2003).
- [30] Lu J., Zhao X. *Int J Modern Phys B*, **16**, 2521 (2002) .
- [31] Moreale A., Closs P., Badot C., *Clay Miner*, **20**, 29 (1985) .
- [32] Chang T.-C., Ho S.-Y., Chao K.-J., *J Chin Chem Soc*, **39**, 209 (1992).
- [33] Carrado K. A., Xu L., *Chem Mater*, **10**, 1440 (1998).
- [34] Kim B. H., Jung J. H., Hong S. H., kim J. W., Choi H. J., Joo J., *Current Appl Phys*, **1**, 112 (2001).
- [35] Silverstein R., Bassler G. and Morrill T., *Spectrometric Identification of Organic Compounds* John Wiley&Sons Inc.New York (1967).
- [36] Colthup N., Daly L., Wiberley S., *Introduction to Infrared and Raman Spectroscopy* (3rd edn) Academic Press San Diego, CA, (1990)
- [37] Kornmann X., Lindberg H., Berglund L. A., *Polym*, **42**, 4493 (2001).
- [38] Wu Q., Xue Z., Qi Z., Wang F., *Polym*, **41**, 2029 (2000).
- [39] Porter T. L., Thompson D., Bradley M., Eastman M. P., Hagerman M. E., Attuso J. L., Votava A. E., Bain E. D., *J Vac Sci Technol A*, **15**, 500 (1997).
- [40] Kelly P., Akelah A., Qutubuddin S., Moet A., *J Mater Sci*, **29** (9), 2274 (1994).
- [41] Chan H. S. O., Ng S. C., Sim W. S., Tan K. L., Tan B. T. G., *Macromolecules*, **25**, 6029 (1992).
- [42] Wei J., Jang G., Hsueh K. F., *Polym Mater Sci Eng*, **61**, 916 (1989).

## FIGURES CAPTIONS

- Fig. (1).** IR spectra of PANI, D<sub>230</sub>-MMT (I), and PANI/D<sub>230</sub>-MMT nanocomposites (I<sub>a-d</sub>) in the region of 3500–500 cm<sup>-1</sup>.
- Fig. (2).** XRD pattern of PANI, D<sub>230</sub>-MMT (I), and PANI/D<sub>230</sub>-MMT nanocomposites (I<sub>a-d</sub>).
- Fig. (3)** XRD pattern of PANI, T<sub>403</sub>-MMT (II), and PANI/T<sub>403</sub>-MMT nanocomposites(II<sub>a-d</sub>).
- Fig. (4)** XRD pattern of PANI, ED<sub>600</sub>-MMT (III), and PANI/ED<sub>600</sub>-MMT nanocomposites (III<sub>a-d</sub>).
- Fig. (5)** XRD pattern of PANI, ED<sub>900</sub>-MMT (IV), and PANI/ED<sub>900</sub>-MMT nanocomposites(IV<sub>a-d</sub>).

- Fig. (6).** TEM images of PANI/D<sub>230</sub>-MMT nanocomposites using (a) 2 wt % of D<sub>230</sub>/MMT; (b) 50 wt % of D<sub>230</sub>/MMT.
- Fig. (7).** SEM images of (a) PANI, (b) PANI/D<sub>230</sub>-MMT at 2 wt % of D<sub>230</sub>- MMT, (c) PANI/D<sub>230</sub>- MMT at 50 wt % of D<sub>230</sub>-MMT.
- Fig. (8).** IR spectra of D<sub>230</sub>-MMT, PANI, PANI/D<sub>230</sub>-MMT (I<sub>b</sub>) nanocomposites, EP, PANI/D<sub>230</sub>-MMT/EP (I<sub>h</sub>, II<sub>i</sub>) nanocomposites.
- Fig. (9).** DSC of (a) PANI/EP and (b) PANI/D<sub>230</sub>-MMT/EP (I<sub>h</sub>).
- Fig. (10).** XRD pattern of D<sub>230</sub>-MMT, PANI/D<sub>230</sub>-MMT nanocomposites, PANI/EP and PANI/D<sub>230</sub>-MMT/EP nanocomposites (I<sub>h</sub>, II<sub>i</sub>).
- Fig. (11).** TEM images of PANI/D<sub>230</sub>-MMT/EP (I<sub>h</sub>) at different magnifications.
- Fig.(12).** (a) TGA curves of PANI, D<sub>230</sub>-MMT (I), PANI/D<sub>230</sub>-MMT nanocomposites containing 25 wt% (I<sub>c</sub>), 50 wt % (I<sub>d</sub>) of D<sub>230</sub>-MMT; (b) PANI/organoclay nanocomposites at 14 wt % of T<sub>403</sub>-MMT (II<sub>b</sub>), ED<sub>600</sub>-MMT (III<sub>b</sub>), ED<sub>900</sub>-MMT(IV<sub>b</sub>).
- Fig. (13).** Electrical conductivity of PANI/organoclay nanocomposites at different concentrations of PANI using (a) D<sub>230</sub>-MMT, (b) T<sub>403</sub>-MMT, (c) ED<sub>600</sub>-MMT and (d) ED<sub>900</sub>-MMT.
- Table (1)** Composition and X-ray data of organoclay
- Table (2)** Composition data of organoclay/PANI nanocomposites
- Table (3)** Composition data of PANI/EP and PANI/D<sub>230</sub>-MMT/EP nanocomposites and electrical conductivity

**Table (1)** Composition and X-ray data of organoclay

Code	Jeffamine		MMT	Organoclay			
	Type	wt (g)	wt (g)	Yield		X-ray data	
				wt (g)	wt (%)	2 $\theta$	d-spacing (Å)
I	D <sub>230</sub>	2.8	10	7.13	55.7	6.3	14
II	T <sub>403</sub>	3.7	10	8.00	58.4	6.0	14.7
III	ED <sub>600</sub>	7.1	10	8.82	57.4	5.1	17.3
IV	ED <sub>900</sub>	11	10	10.44	49.7	5.0	17.6

**Table (2)** Composition data of organoclay/PANI nanocomposites

code	Ratio (wt%)	Organoclay		PANI	
		Type	wt (g)	Aniline wt	APS wt
I <sub>a</sub>	2%	D <sub>230</sub> -MMT	0.0183	0.9	2.2
I <sub>b</sub>	14%	D <sub>230</sub> -MMT	0.146	0.9	2.2
I <sub>c</sub>	25%	D <sub>230</sub> -MMT	0.3	0.9	2.2
I <sub>d</sub>	50%	D <sub>230</sub> -MMT	0.9	0.9	2.2
II <sub>a</sub>	2%	T <sub>403</sub> -MMT	0.0183	0.9	2.2
II <sub>b</sub>	14%	T <sub>403</sub> -MMT	0.146	0.9	2.2
II <sub>c</sub>	25%	T <sub>403</sub> -MMT	0.3	0.9	2.2
II <sub>d</sub>	50%	T <sub>403</sub> -MMT	0.9	0.9	2.2
III <sub>a</sub>	2%	ED <sub>600</sub> -MMT	0.0183	0.9	2.2
III <sub>b</sub>	14%	ED <sub>600</sub> -MMT	0.146	0.9	2.2
III <sub>c</sub>	25%	ED <sub>600</sub> -MMT	0.3	0.9	2.2
III <sub>d</sub>	50%	ED <sub>600</sub> -MMT	0.9	0.9	2.2
IV <sub>a</sub>	2%	ED <sub>900</sub> -MMT	0.0183	0.9	2.2
IV <sub>b</sub>	14%	ED <sub>900</sub> -MMT	0.146	0.9	2.2
IV <sub>c</sub>	25%	ED <sub>900</sub> -MMT	0.3	0.9	2.2
IV <sub>d</sub>	50%	ED <sub>900</sub> -MMT	0.9	0.9	2.2

**Table (3)** Composition data of PANI/EP and PANI/D<sub>230</sub>-MMT/EP nanocomposites and electrical conductivity

Code	EP (g)	Curing agent		Calcinations	Conductivity S/cm
		Type	wt (g)	Residue (wt%)	
PANI/EP	2	PANI	2	1.898	<10 <sup>-9</sup>
I <sub>h</sub>	1	PANI/D <sub>230</sub> -MMT(I <sub>b</sub> )	1.5	2.9	2.1x10 <sup>-7</sup>
II <sub>i</sub>	1	PANI/D <sub>230</sub> -MMT(I <sub>b</sub> )	0.6	2	3.2x10 <sup>-7</sup>

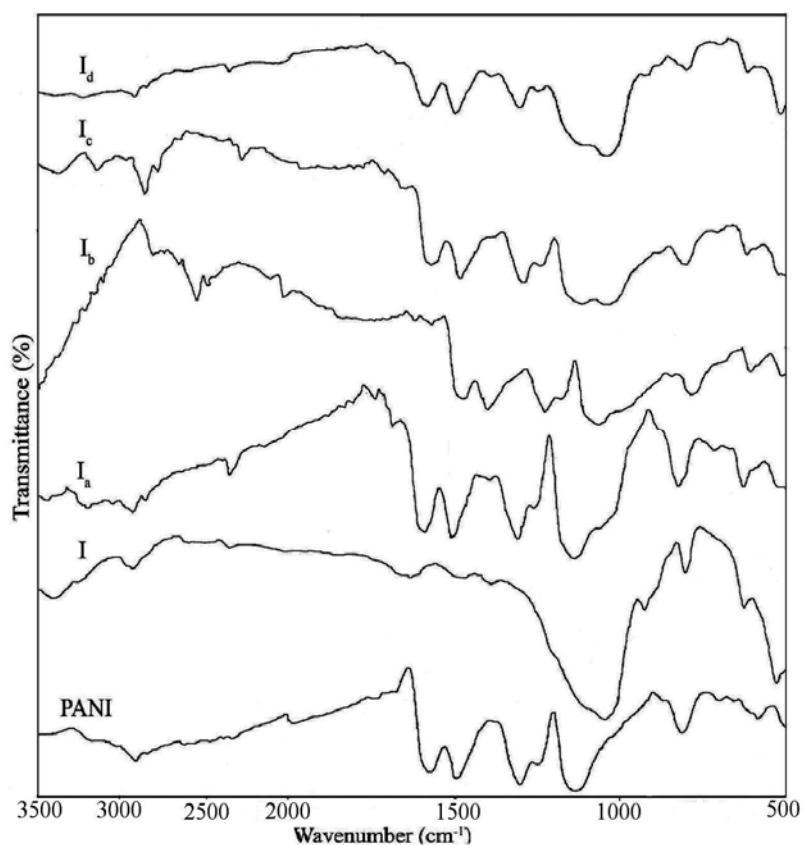


**Fig. (1).** IR spectra of PANI, D<sub>230</sub>-MMT (I), and PANI/D<sub>230</sub>-MMT nanocomposites (I<sub>a-d</sub>) in the region of 3500–500 cm<sup>-1</sup>.

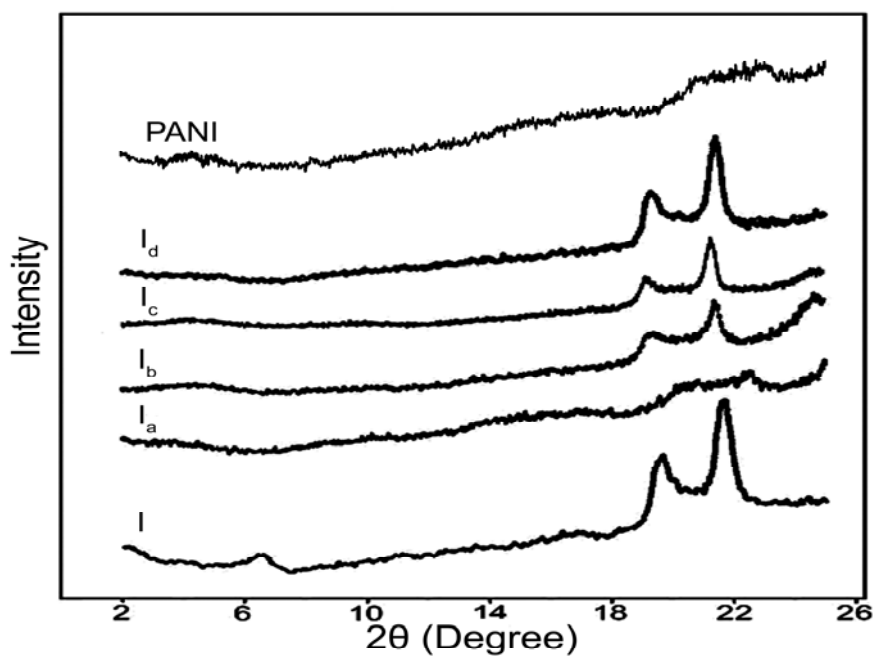


**Fig. (2).** XRD pattern of PANI, D<sub>230</sub>-MMT (I), and PANI/D<sub>230</sub>-MMT nanocomposites (I<sub>a-d</sub>).

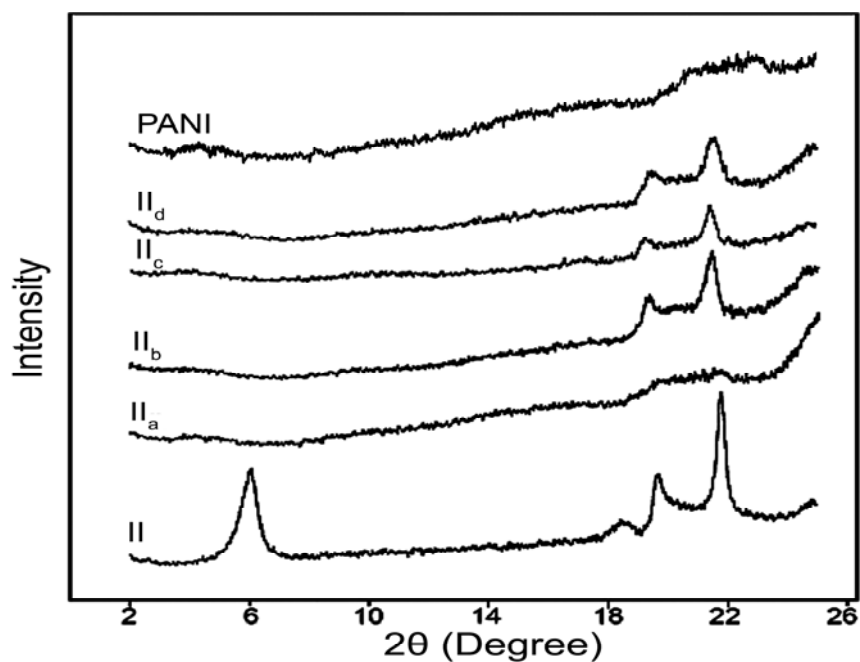


**Fig. (3)** XRD pattern of PANI, T<sub>403</sub>-MMT (II), and PANI/T<sub>403</sub>-MMT nanocomposites(II<sub>a-d</sub>).

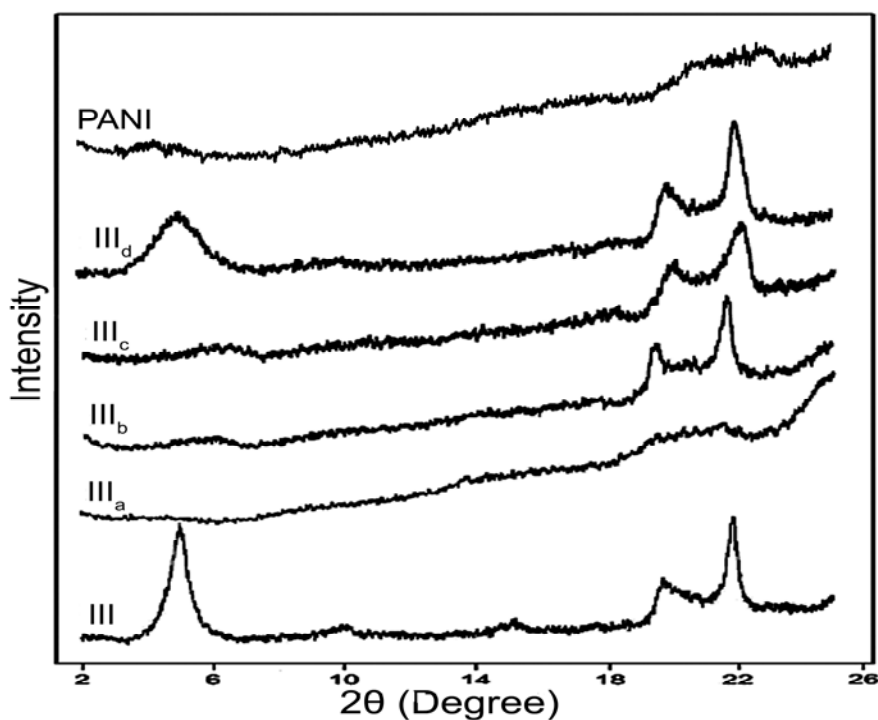


**Fig. (4)** XRD pattern of PANI, ED<sub>600</sub>-MMT (III), and PANI/ED<sub>600</sub>-MMT nanocomposites (III<sub>a-d</sub>).

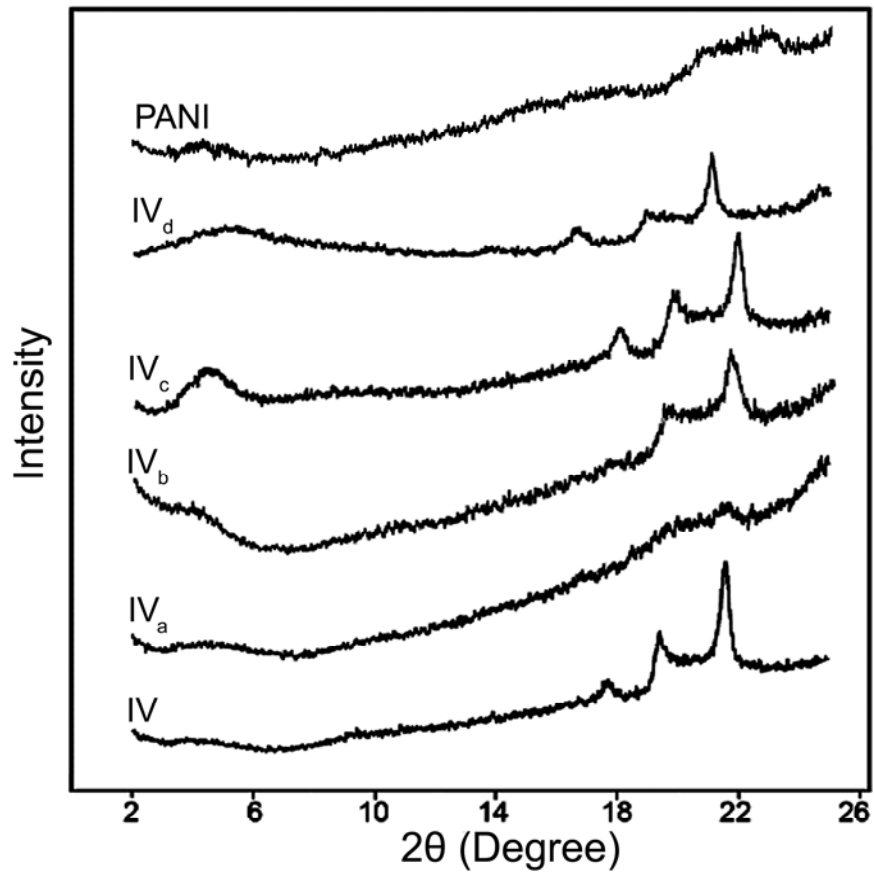


**Fig.(5)** XRD pattern of PANI, ED<sub>900</sub>-MMT (IV), and PANI/ED<sub>900</sub>-MMT nanocomposites(IV<sub>a-d</sub>).

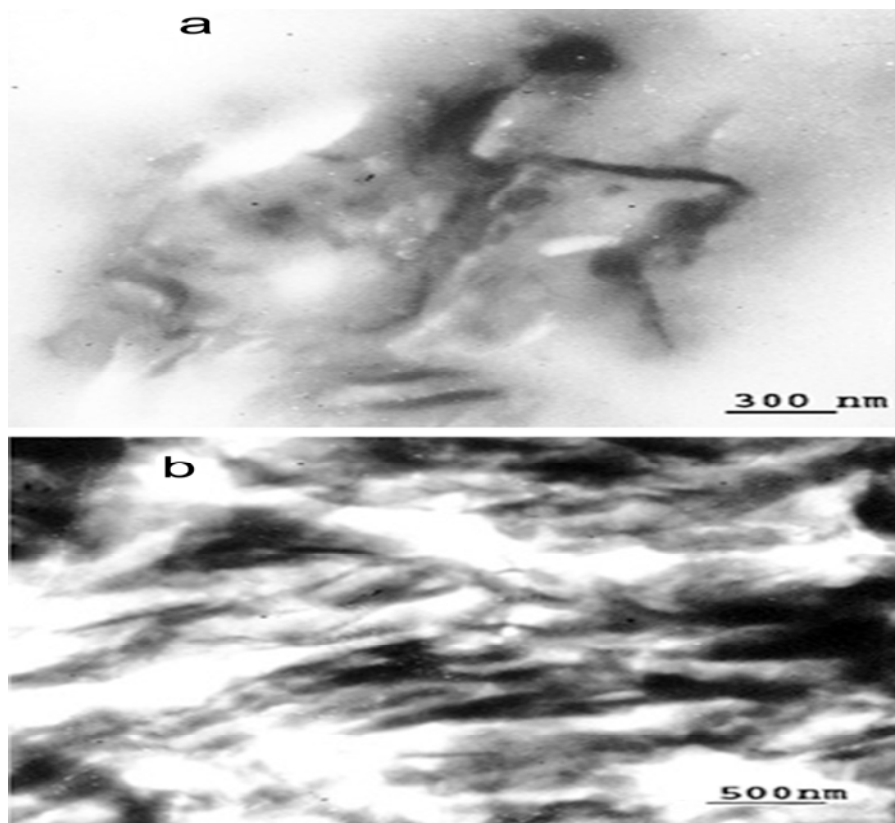


**Fig. (6)** TEM images of PANI/D<sub>230</sub>-MMT nanocomposites using (a) 2 wt % of D<sub>230</sub>/MMT; (b) 50 wt % of D<sub>230</sub>/MMT.

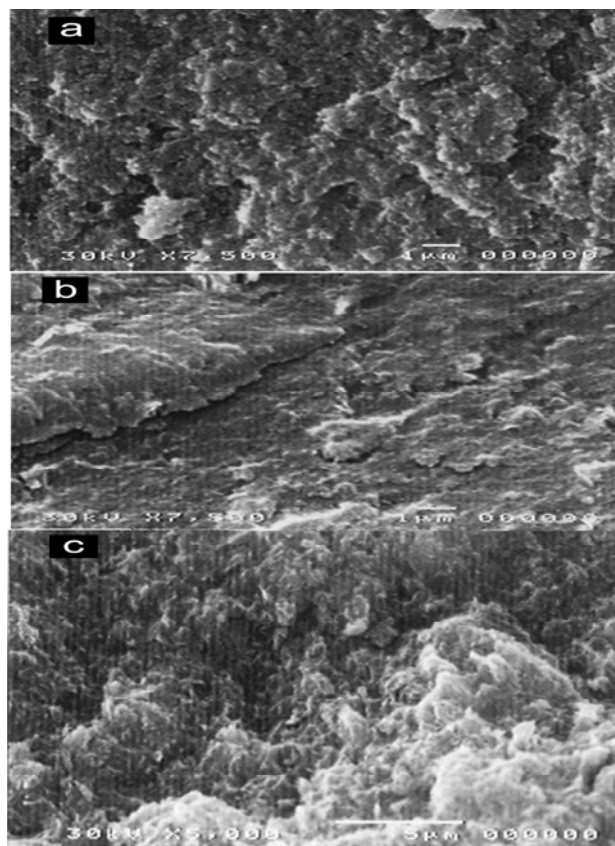


**Fig. (7)** SEM images of (a) PANI, (b) PANI/D<sub>230</sub>-MMT at 2 wt % of D<sub>230</sub>- MMT, (c) PANI/D<sub>230</sub>- MMT at 50 wt % of D<sub>230</sub>-MMT.

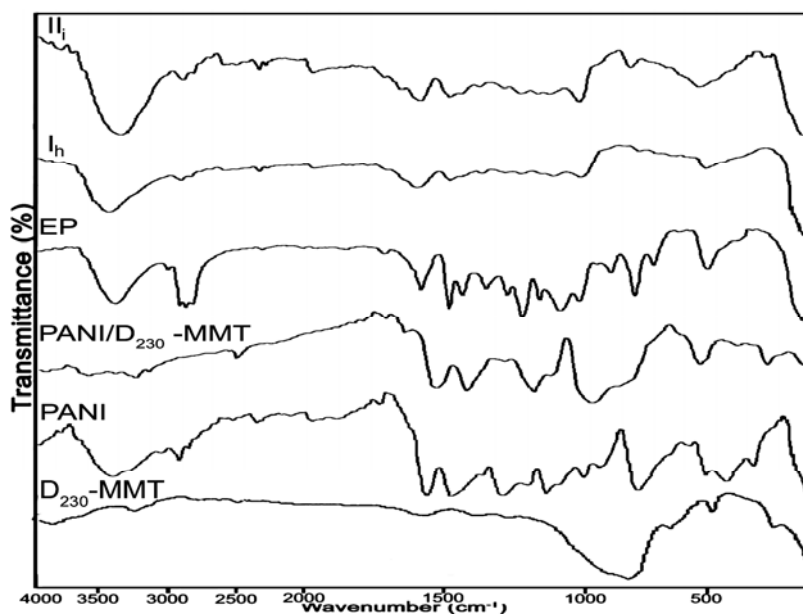


**Fig. (8)** IR spectra of D<sub>230</sub>-MMT, PANI, PANI/D<sub>230</sub>-MMT (I<sub>b</sub>) nanocomposites, EP, PANI/D<sub>230</sub>-MMT/EP (I<sub>h</sub>, II<sub>i</sub>) nanocomposites.

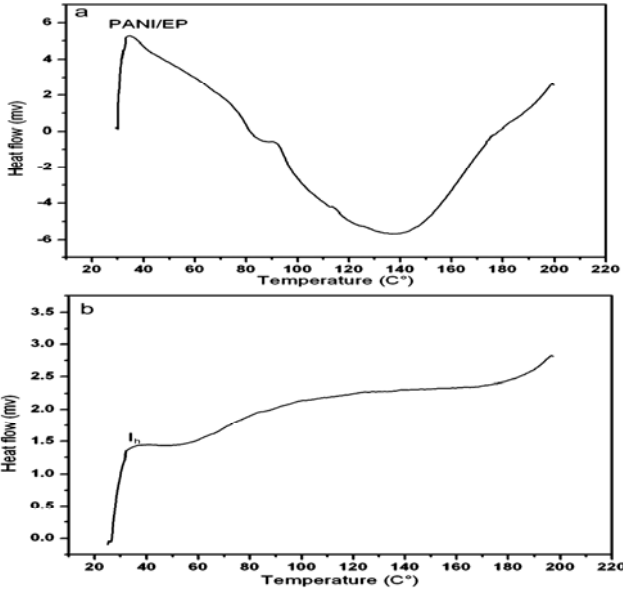


Fig. (9). DSC of (a) PANI/EP and (b) PANI/D<sub>230</sub>-MMT/EP (I<sub>h</sub>).

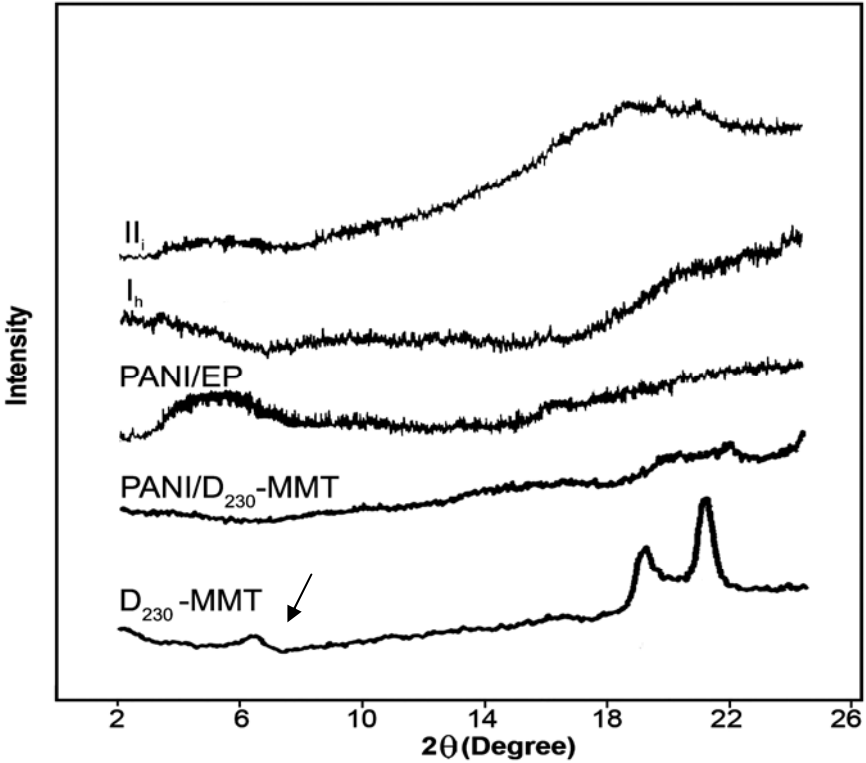
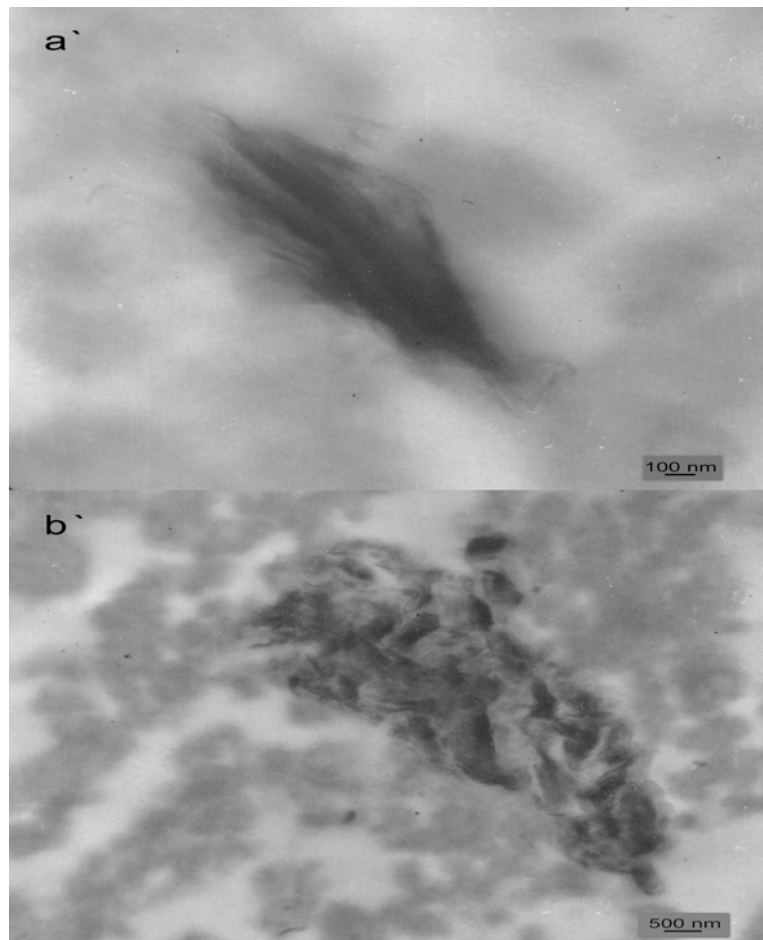
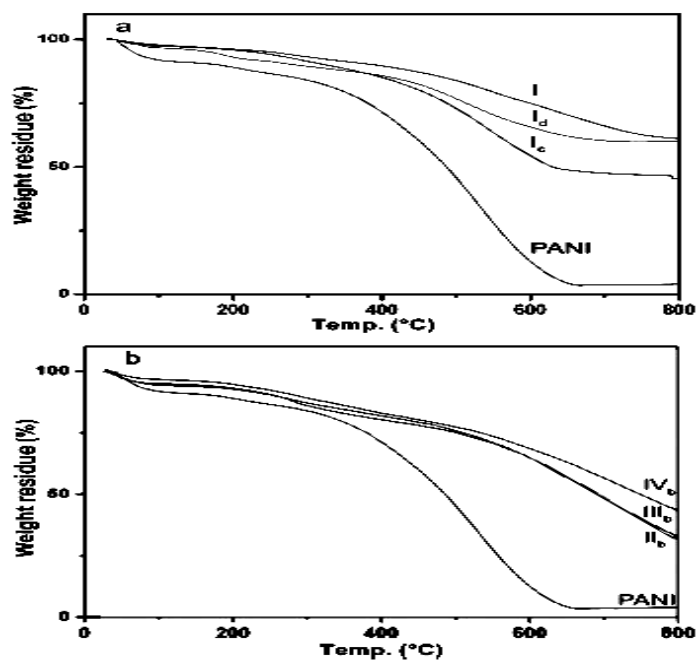


Fig. (10) XRD pattern of D<sub>230</sub>-MMT, PANI/D<sub>230</sub>-MMT nanocomposites, PANI/EP and PANI/D<sub>230</sub>-MMT/EP nanocomposites (I<sub>h</sub>, II<sub>i</sub>).



**Fig. (11)** TEM images of PANI/D<sub>230</sub>-MMT/EP (I<sub>h</sub>) at different magnifications.



**Fig. (12).** (a) TGA curves of PANI, D<sub>230</sub>-MMT (I), PANI/D<sub>230</sub>-MMT nanocomposites containing 25 wt% (I<sub>c</sub>), 50 wt % (I<sub>d</sub>) of D<sub>230</sub>-MMT; (b) PANI/organoclay nanocomposites at 14 wt % of T<sub>403</sub>-MMT (II<sub>b</sub>), ED<sub>600</sub>-MMT (III<sub>b</sub>), ED<sub>900</sub>-MMT(IV<sub>b</sub>)

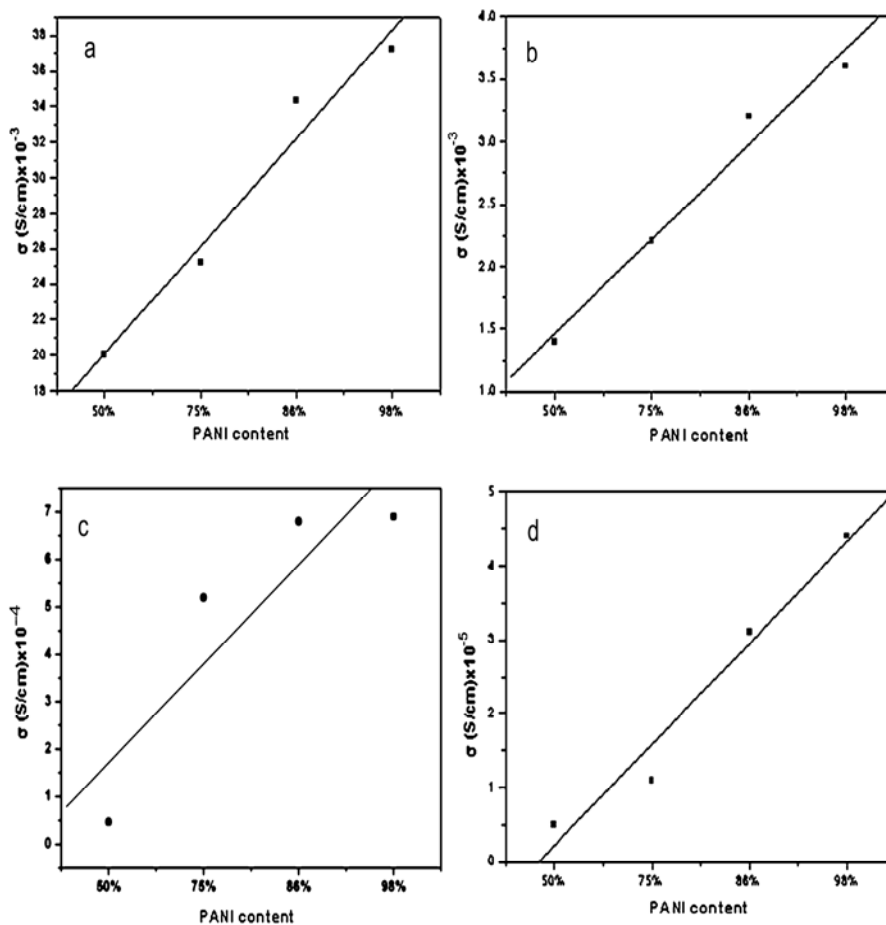


**Fig. (13)** Electrical conductivity of PANI/organoclay nanocomposites at different concentrations of PANI using (a) D<sub>230</sub>-MMT, (b) T<sub>403</sub>-MMT, (c) ED<sub>600</sub>-MMT and (d) ED<sub>900</sub>-MMT.